Appl. Math. Mech. -Engl. Ed., **38**(7), 969–980 (2017)
DOI 10.1007/s10483-017-2219-6

Applied Mathematics and Mechanics (English Edition)

Nonlinear three-dimensional stretched flow of an Oldroyd-B fluid with convective condition, thermal radiation, and mixed convection*

B. MAHANTHESH[1,2], B. J. GIREESHA[2], S. A. SHEHZAD[3,†], F. M. ABBASI[4], R. S. R. GORLA[5]

1. Department of Mathematics, Christ University, Bangalore 560029, Karnataka, India;
2. Department of Studies and Research in Mathematics, Kuvempu University, Shankarghatta 577451, Karnataka, India;
3. Department of Mathematics, COMSATS Institute of Information Technology, Sahiwal 57000, Pakistan;
4. Department of Mathematics, COMSATS Institute of Information Technology, Islamabad 44000, Pakistan;
5. Department of Mechanical and Civil Engineering, Purdue University Northwest, Indiana 46391, U. S. A.

Abstract The effect of non-linear convection in a laminar three-dimensional Oldroyd-B fluid flow is addressed. The heat transfer phenomenon is explored by considering the non-linear thermal radiation and heat generation/absorption. The boundary layer assumptions are taken into account to govern the mathematical model of the flow analysis. Some suitable similarity variables are introduced to transform the partial differential equations into ordinary differential systems. The Runge-Kutta-Fehlberg fourth- and fifth-order techniques with the shooting method are used to obtain the solutions of the dimensionless velocities and temperature. The effects of various physical parameters on the fluid velocities and temperature are plotted and examined. A comparison with the exact and homotopy perturbation solutions is made for the viscous fluid case, and an excellent match is noted. The numerical values of the wall shear stresses and the heat transfer rate at the wall are tabulated and investigated. The enhancement in the values of the Deborah number shows a reverse behavior on the liquid velocities. The results show that the temperature and the thermal boundary layer are reduced when the non-linear convection parameter increases. The values of the Nusselt number are higher in the non-linear radiation situation than those in the linear radiation situation.

Key words nonlinear thermal convection, nonlinear thermal radiation, Oldroyd-B fluid, convective boundary condition, heat source/sink

Chinese Library Classification O361
2010 Mathematics Subject Classification 76A05

* Received Dec. 14, 2016 / Revised Mar. 17, 2017
† Corresponding author, E-mail: ali_qau70@yahoo.com

1 Introduction

The complex nature of non-Newtonian fluids has posed interesting mathematical challenges for mathematicians, engineers, and researchers. This is because that non-Newtonian fluids play a vital role in the applications of physiology, biology, and industry. Common examples of such a type of applications include blood, shampoos, sauces, drilling muds, certain oils, lubricants, polymer solutions, and colloidal suspensions. The simple constitutive expression of Navier-Stokes is incapable to predict the mechanism of all such materials. This fact leads to the development of various non-Newtonian fluid models according to their physical nature. Here, we adopt the Oldroyd-B fluid model, which falls into the category of the rate type non-Newtonian liquids. The main feature of the Oldroyd-B fluid is to characterize the nature of the stress relaxation and retardation, which cannot be explored by the Maxwell fluid model. The idea of the boundary layer flow of the Oldroyd-B liquid induced by the linear stretching of a surface was first initiated by Sajid et al.[1]. They reported the two-dimensional boundary layer flow of an Oldroyd-B liquid near a stagnation point, and developed the numerical solutions of the governing flow expressions. Many investigators have extended the work of Sajid et al.[1]. Shehzad et al.[2] discussed the effects of the temperature-dependent thermal conductivity on the three-dimensional flow of the Oldroyd-B fluid model, and considered that the flow generation was due to the bidirectional stretching of the surface. Hayat et al.[3] addressed the effects of the temperature stratification in a steady-state stagnation point of the Oldroyd-B liquid with mixed convection, and developed the homotopic expressions of the solutions for velocity and temperature. Motsa et al.[4] developed a spectral relaxation technique for the temperature-dependent three-dimensional flow of the Oldroyd-B liquid with heat source/sink effects. Abbasi et al.[5] discussed the Cattaneo-Christov heat flux theory for the steady flow of the Oldroyd-B fluid over a moving sheet, and obtained the velocity and temperature by employing the optimal homotopic algorithm.

The thermal convection problems of fluid flows are very prominent in a number of industrial, engineering, and energy storage processes. Sheikholeslami et al.[6] employed the lattice-Boltzmann technique to analyze the problem of the natural convection flow of a viscous nanoliquid under applied magnetic field. They considered the Cu-water nanoparticles filled in an annulus. Sheikholeslami et al.[7] analyzed the forced convection non-uniform magnetohydrodynamic flow of a nanoliquid in a lid driven annulus. Mahanthesh et al.[8] studied the mixed convective squeezing flow of a three-dimensional viscous nanofluid filled in a rotating channel, and presented numerical computations to examine the effects of various pertinent parameters. Rashidi et al.[9] discussed the effects of mixed convection on the hydromagnetic flow of the Al_2O_3-water nanoliquid induced by a channel with sinusoidal walls and heat transfer. Abbasi et al.[10] developed the homotopic algorithm to analyze the effects of double stratification in the mixed convective flow of the Maxwell nanoliquid over a moving surface with heat generation/absorption. Some recent investigations on convective flows can be found in Refs. [11]–[15].

Thermally radiative flows are generally encountered when the difference between the ambient temperature and the surface of the sheet is high. In several industrial processes, the thermal boundary layer thickness can be changed by use of thermal radiation. Examples of such industrial processes include nuclear reactors, power plants, satellites, missiles technology, gas turbines, etc. Abundant studies have been carried out in the literatures to predict the effects of thermal radiation (see Refs. [16]–[25] and the references therein). In these studies, the authors utilized the Rosseland approximations to linearize the thermal radiation term. In recent years, the investigation on non-linear thermal radiation has become a hot spot research topic. Cortell[26] addressed the effects of the non-linear thermally radiative heat transfer in the steady laminar flow of a viscous liquid over a linear sheet. Mushtaq et al.[27] analyzed the solar radiation effects in the two-dimensional flow of a viscous fluid, and presented a numerical analysis by taking the Brownian motion and thermophoretic effects into consideration. Shehzad et al.[28]

reported the non-linear thermal radiation effect in the three-dimensional Jeffrey nanoliquid over a bidirectional stretching surface. Hayat et al.[29] reported the hydromagnetic three-dimensional viscoelastic fluid flow with non-linear thermal radiation. Mahanthesh et al.[30] addressed the water-based nanofluid flow induced by the non-linear stretching surface under the effects of applied magnetic field and thermal radiation.

In this attempt, our main concern is to introduce the non-linear convection in the three-dimensional flow of an Oldroyd-B fluid induced by the stretching of the bidirectional stretching surface. We also consider the nonlinear thermal radiation and heat generation/absorption effects in the heat transfer expressions. The convective condition is employed at the boundary surface instead of the constant surface temperature condition. Different problems of the fluid flows have been treated by various numerical techniques[31–40]. The present mathematical model is tackled through the fourth- and fifth-order formulae of the Runge-Kutta-Fehlberg techniques via the shooting algorithm. The results are plotted for multiple values of the dimensionless parameters to examine the curves of the velocities and temperature. The results are also discussed for the case of linear thermal radiation.

2 Flow and heat transfer analysis

The non-linear convection in an Oldroyd-B fluid past a stretching sheet is considered. A steady boundary layer flow is induced by the stretched surface at $z = 0$, and it occupies the region $z > 0$. The sheet is stretched in two directions with the velocities $u_w = ax$ and $v_w = by$ along the x- and y-directions correspondingly. We assume that T_f is the temperature of the convective surface, and T_∞ is the ambient fluid temperature. The magnetic Reynolds number is assumed to be so small that the induced magnetic field and the Hall current are negligible. The mathematical expressions of the conservation laws of mass, momentum, and energy subjected to the boundary layer assumptions are

$$\frac{\partial u}{\partial x} + \frac{\partial v}{\partial y} + \frac{\partial w}{\partial z} = 0, \tag{1}$$

$$\begin{aligned}
&u\frac{\partial u}{\partial x} + v\frac{\partial u}{\partial y} + w\frac{\partial u}{\partial z} \\
&\quad + \lambda_1\Big(u^2\frac{\partial^2 u}{\partial x^2} + v^2\frac{\partial^2 u}{\partial y} + w^2\frac{\partial^2 u}{\partial z^2} + 2uv\frac{\partial^2 u}{\partial x\partial y} + 2vw\frac{\partial^2 u}{\partial y\partial z} + 2uw\frac{\partial^2 u}{\partial x\partial z}\Big) \\
&= \nu\Big(\frac{\partial^2 u}{\partial z^2} + \lambda_2\Big(u\frac{\partial^3 u}{\partial x\partial z^2} + v\frac{\partial^3 u}{\partial y\partial z^2} + w\frac{\partial^3 u}{\partial z^3} - \frac{\partial u\partial^2 u}{\partial x\partial z^2} - \frac{\partial u\partial^2 v}{\partial y\partial z^2} - \frac{\partial u\partial^2 w}{\partial z\partial z^2}\Big)\Big) \\
&\quad + g(\beta_0(T - T_\infty) + \beta_1(T - T_\infty)^2),
\end{aligned} \tag{2}$$

$$\begin{aligned}
&u\frac{\partial v}{\partial x} + v\frac{\partial v}{\partial y} + w\frac{\partial v}{\partial z} \\
&\quad + \lambda_1\Big(u^2\frac{\partial^2 v}{\partial x^2} + v^2\frac{\partial^2 v}{\partial y} + w^2\frac{\partial^2 v}{\partial z^2} + 2uv\frac{\partial^2 v}{\partial x\partial y} + 2vw\frac{\partial^2 v}{\partial y\partial z} + 2uw\frac{\partial^2 v}{\partial x\partial z}\Big) \\
&= \nu\Big(\frac{\partial^2 v}{\partial z^2} + \lambda_2\Big(u\frac{\partial^3 v}{\partial x\partial z^2} + v\frac{\partial^3 u}{\partial y\partial z^2} + w\frac{\partial^3 u}{\partial z^3} - \frac{\partial v\partial^2 v}{\partial x\partial z^2} - \frac{\partial v\partial^2 v}{\partial y\partial z^2} - \frac{\partial v\partial^2 w}{\partial z\partial z^2}\Big)\Big),
\end{aligned} \tag{3}$$

$$u\frac{\partial T}{\partial x} + v\frac{\partial T}{\partial y} + w\frac{\partial T}{\partial z} = \alpha_m\frac{\partial^2 T}{\partial z^2} + \frac{Q_0}{\rho C_p}(T - T_\infty) - \frac{1}{\rho C_p}\frac{\partial q_r}{\partial z}, \tag{4}$$

where u, v, and w are, respectively, the velocity components along the x-, y-, and z-directions, T is the temperature, λ_1 is the relaxation time, λ_2 is the retardation time, ν is the kinematic viscosity, g is the acceleration due to gravity, β_0 and β_1 are the volumetric thermal expansion coefficients, $\alpha_m = k/(\rho C_p)$ is the thermal diffusivity of the fluid, k is the thermal conductivity, ρ is the fluid density, C_p is the fluid specific heat, Q_0 is the heat generation/absorption coefficient, and q_{r} is the radiative heat flux. The present flow analysis is reduced to the Maxwell model by setting $\lambda_2 = 0$. Further, this analysis can be recovered for viscous liquids when $\lambda_1 = 0 = \lambda_2$.

The thermal radiation heat flux expression through the Rosseland approximation is[29]

$$q_{\mathrm{r}} = -\frac{4}{3k_1}\nabla e_{\mathrm{b}}, \tag{5}$$

where k_1 is the mean absorption coefficient, $e_{\mathrm{b}} = \sigma T^4$ is the rate of the radiation emitted per square meter of surface, and σ is the Stefan-Boltzmann constant. The definition of e_{b} is through the Stefan-Boltzmann law, which states that all the objects with the temperature above absolute zero emit radiations at the rate proportional to the fourth power of its absolute temperature.

In view of Eq. (5), we have

$$\begin{aligned} &u\frac{\partial T}{\partial x} + v\frac{\partial T}{\partial y} + w\frac{\partial T}{\partial z} \\ &= \frac{\partial}{\partial z}\Big(\Big(\alpha_m + \frac{16\sigma^*}{3\rho k_1 C_p}T^3\Big)\frac{\partial T}{\partial z}\Big) + \frac{Q_0}{\rho C_p}(T - T_\infty). \end{aligned} \tag{6}$$

The relevant boundary conditions for the present problem are

$$\begin{cases} u = u_w, \quad v = v_w, \quad w = 0, \quad k\dfrac{\partial T}{\partial z} = h_f(T - T_f) \quad \text{at} \quad z = 0, \\ u \to 0, \quad v \to 0, \quad \dfrac{\partial u}{\partial z} \to 0, \quad \dfrac{\partial v}{\partial z} \to 0, \quad T \to T_\infty \quad \text{as} \quad z \to \infty. \end{cases} \tag{7}$$

The governing partial differential equations suggest transformation into the corresponding non-linear ordinary differential equations by choosing the following similarity variables[28–29]:

$$\begin{cases} u = axf'(\eta), \quad v = byg'(\eta), \quad w = -\sqrt{\nu a}(f(\eta) + g(\eta)), \\ T = T_\infty + \theta(\eta)(T_f - T_\infty), \quad \eta = \sqrt{\dfrac{a}{\nu}}z, \end{cases} \tag{8}$$

where a prime denotes differentiation with respect to η. In view of the above relations, we obtain the following set of non-linear ordinary differential equations:

$$\begin{aligned} &f''' + (f+g)f'' - f'^2 + \beta_1(2(f+g)f'f'' - (f+g)^2 f''') \\ &+ \beta_2((f'' + g'')f'' - (f+g)f'''') + \lambda(1 + \gamma\theta)\theta = 0, \end{aligned} \tag{9}$$

$$\begin{aligned} &g''' + (f+g)g'' - g'^2 + \beta_1(2(f+g)g'g'' - (f+g)^2 g''') \\ &+ \beta_2((f'' + g'')g'' - (f+g)g'''') = 0, \end{aligned} \tag{10}$$

$$\frac{1}{Pr}((1 + Rd(1 + (\theta_w - 1)\theta)^3)\theta')' + (f+g)\theta' + S\theta = 0. \tag{11}$$

The boundary conditions for the present flow problem are

$$\begin{cases} f'(\eta) = 1, \quad g'(\eta) = c, \quad f(\eta) = 0, \\ g(\eta) = 0, \quad \theta'(\eta) = Bi(\theta(\eta) - 1) \quad \text{at} \quad \eta = 0, \end{cases} \tag{12}$$

$$f' \to 0, \quad f'' \to 0, \quad g' \to 0, \quad g'' \to 0, \quad \theta \to 0 \quad \text{as} \quad \eta \to 0, \tag{13}$$

where the dimensionless parameters are

$$\begin{cases} \beta_1 = \lambda_1 a, \quad \beta_2 = \lambda_2 a, \quad c = \dfrac{b}{a}, \quad \lambda = \dfrac{Gr_x}{Re_x^2}, \quad Re_x = \dfrac{x u_w}{\nu}, \quad Gr_x = \dfrac{g_v \beta_0 (T_f - T_\infty) x^3}{\nu^2}, \\ \gamma = \dfrac{\beta_1 (T_f - T_\infty)}{\beta_0}, \quad R = \dfrac{16\sigma T_\infty^3}{3k_1 k}, \quad \theta_w = \dfrac{T_f}{T_\infty}, \quad S = \dfrac{Q_0}{a\rho C_p}, \quad Pr = \dfrac{\mu C_p}{k}, \quad Bi = \dfrac{h_f}{k\sqrt{\nu/a}}. \end{cases}$$

In the above equations, β_1 and β_2 are the Deborah numbers, c is the stretching ratio parameter, λ is the mixed convection parameter, Re_x is the Reynolds number, Gr_x is the Grashof number, γ is the non-linear convection parameter, R is the thermal radiation parameter, θ_w is the temperature ratio parameter, S is the heat source/sink parameter, Pr is the Prandtl number, and Bi is the Biot number.

The engineering interested physical quantity of the boundary value problems is the local Nusselt number Nu, which is defined by

$$Nu = \frac{u_w q_w}{ak(T_f - T_\infty)}, \tag{14}$$

where q_w is the surface heat flux. With the similarity variables, we obtain

$$\frac{Nu}{\sqrt{Re_x}} = -(1 + R\theta_w^3)\theta'(0). \tag{15}$$

Since the exact solution of the complicated nonlinear boundary value problem presented by Eqs. (9)–(13) is impracticable, we intend to handle this problem numerically.

3 Numerical analysis

The nonlinear boundary value problem is solved numerically by use of the Runge-Kutta-Fehlberg method along with the shooting technique. First, the non-linear differential equations are discretized to ten first-order linear differential equations. Then, the unknown initial conditions are calculated by use of the iterative technique, i.e., the shooting method, with some appropriate initial guesses. The fourth- and fifth-order formulae of the Runge-Kutta-Fehlberg method are[18,30]

$$\overline{y}_{m+1} = \overline{y}_m + h\Big(\frac{25}{216}k_0 + \frac{1\,408}{2\,565}k_2 + \frac{2\,197}{4\,109}k_3 - \frac{1}{5}k_4\Big), \tag{16}$$

$$\overline{y}_{m+1} = \overline{y}_m + h\Big(\frac{16}{135}k_0 + \frac{6\,656}{12\,825}k_2 + \frac{28\,561}{56\,430}k_3 - \frac{9}{50}k_4 + \frac{2}{55}k_5\Big), \tag{17}$$

where

$$\begin{cases} k_0 = f\Big(\overline{x}_m, \overline{y}_m\Big), \\ k_1 = f\Big(\overline{x}_m + \dfrac{h}{4}, \overline{y}_m + \dfrac{hk_0}{4}\Big), \\ k_2 = f\Big(\overline{x}_m + \dfrac{3}{8}h, \overline{y}_m + \Big(\dfrac{3}{32}k_0 + \dfrac{9}{32}k_1\Big)h\Big), \\ k_3 = f\Big(\overline{x}_m + \dfrac{12}{13}h, \overline{y}_m + \Big(\dfrac{1\,932}{2\,197}k_0 - \dfrac{7\,200}{2\,197}k_1 + \dfrac{7\,296}{2\,197}k_2\Big)h\Big), \\ k_4 = f\Big(\overline{x}_m + h, \overline{y}_m + \Big(\dfrac{439}{216}k_0 - 8k_1 + \dfrac{3\,860}{513}k_2 - \dfrac{845}{4\,104}k_3\Big)h\Big), \\ k_5 = f\Big(\overline{x}_m + \dfrac{h}{2}, \overline{y}_m + \Big(-\dfrac{8}{27}k_0 + 2k_1 - \dfrac{3\,544}{2\,565}k_2 + \dfrac{1\,859}{4\,104}k_3 - \dfrac{11}{40}k_4\Big)h\Big). \end{cases}$$

The inner iteration is counted until the nonlinear solution converges with a convergence criterion of 10^{-6}. In addition, the step size is set to be $\Delta\eta = 0.001$. Another challenge to solve the system is fixing the appropriate finite values of η_∞. In this study, the asymptotic boundary conditions are replaced by η_8 in such a way that $f'(8) = g'(8) = f''(8) = g''(8) = \theta(8) = 0$. This ensures that all numerical solutions approach the asymptotic values correctly. In order to check the accuracy of our numerical method, the values of $-f''(0)$ and $-g''(0)$ for different values of the stretching ratio parameter are compared with those of Ref. [41], where the numerical results are obtained by the homotopy perturbation method (HPM) and the obtained exact solutions are for Newtonian fluids, when $\lambda = R = 0$. The results are presented in Table 1. From the table, we can see that the present solutions are in good agreement with those of Ref. [41] as a limiting case.

Table 1 Results of $-f''(0)$ and $-g''(0)$ for different values of c

c	HPM[41]		Exact[41]		Present	
	$-f''(0)$	$-g''(0)$	$-f''(0)$	$-g''(0)$	$-f''(0)$	$-g''(0)$
0.0	1.000 00	0.000 00	1.000 000	0.000 000	1.000 00	0.000 00
0.1	1.020 25	0.066 84	1.020 259	0.066 847	1.020 26	0.066 85
0.2	1.039 49	0.148 73	1.039 495	0.148 736	1.039 49	0.148 73
0.3	1.057 95	0.243 35	1.057 954	0.243 359	1.057 95	0.243 36
0.4	1.075 78	0.349 20	1.075 788	0.349 208	1.075 78	0.349 20
0.5	1.093 09	0.465 20	1.093 095	0.465 204	1.093 09	0.465 21

4 Discussion

The graphs of the velocity distributions $f'(\eta)$, $g'(\eta)$ and the temperature field $\theta(\eta)$ for multiple values of the Deborah numbers β_1 and β_2, the ratio parameter c, the mixed convective parameter λ, the non-linear convection parameter γ, the radiation parameter R, the heat source/sink parameter S, the Biot number Bi, and the temperature ratio θ_w are visualized in Figs. 1–9.

Figure 1 is presented to explore the effects of the Deborah number β_1 on the velocities $f'(\eta)$, $g'(\eta)$ and the temperature $\theta(\eta)$. From the figure, we can see that, when β_1 increases, the velocities decrease first, then increase when β_1 is large enough. This is because that, the Deborah number β_1 depends on the relaxation time, and the relaxation time enhances for higher β_1. Such an enhancement in the relaxation time leads to lower velocities and higher temperature. It is also observed that the values of $f'(\eta)$ at the wall are higher than those of $g'(\eta)$ and $\theta(\eta)$ at the wall. The effects of β_2 on $f'(\eta)$, $g'(\eta)$, and $\theta(\eta)$ are visualized in Fig. 2.

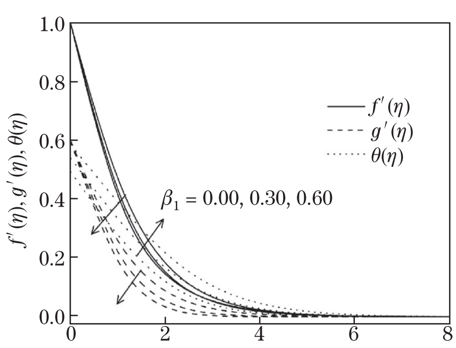

Fig. 1 Curves of $f'(\eta), g'(\eta)$, and $\theta(\eta)$ for various β_1, where $\beta_2 = 0.2$, $\lambda = 0.5$, $Pr = 1.2$, $R = 0.4$, $c = 0.6$, $S = 0.3$, $Bi = 0.4$, and $\theta_w = 1.6$

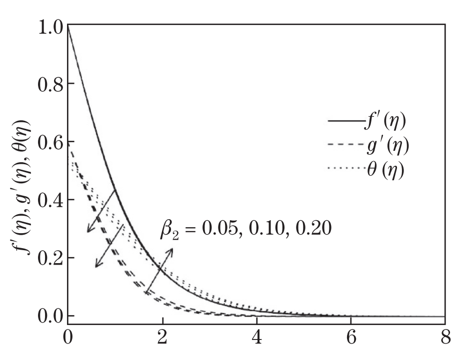

Fig. 2 Curves of $f'(\eta), g'(\eta)$, and $\theta(\eta)$ for various β_2, where $\beta_1 = 0.2$, $\lambda = 0.5$, $Pr = 1.2$, $R = 0.4$, $c = 0.6$, $S = 0.3$, $Bi = 0.4$, and $\theta_w = 1.6$

From this figure, we see that $f'(\eta)$ and $g'(\eta)$ increase when β_2 increases. The variations in $g'(\eta)$ are quite prominent in comparison with the changes in the curves of $f'(\eta)$. Moreover, an increase in β_2 leads to lower temperature and thinner thermal boundary layer. From the definition of β_2, we can see that the retardation factor is higher for larger β_2, which may create decreases in the temperature and the thermal boundary layer. The present results can be modified to the results of the Maxwell fluid by taking $\beta_2 = 0$. The analysis of the three-dimensional flow of the viscous liquid can be retrieved by setting $\beta_1 = 0 = \beta_2$.

The velocity $f'(\eta)$ and the temperature $\theta(\eta)$ decay while the velocity $g'(\eta)$ increases remarkably when c increases (see Fig. 3). It is due to the fact that an increase in c from zero leads to the movement of the lateral surface in the y-direction that corresponds to a higher velocity $g'(\eta)$ and its associated boundary layer thickness. The present three-dimensional problem can be converted into a two-dimensional flow model when $c = 0$. From Fig. 4, we can see that the velocity $f'(\eta)$ increases remarkably while the velocity $g'(\eta)$ and the temperature $\theta(\eta)$ decrease when the mixed convective parameter λ increases. This occurs due to the buoyancy force in λ. The curves of $f'(\eta)$, $g'(\eta)$, and $\theta(\eta)$ for various values of the non-linear convection parameter are given in Fig. 5. Here, the velocity $f'(\eta)$ is an increasing function of the non-linear convection parameter. When γ increases, $g'(\eta)$ and $\theta(\eta)$ decrease.

Figure 6 clearly shows that, when the radiative parameter increases, the values of $f'(\eta)$ and $\theta(\eta)$ become higher, while the values of the velocity $g'(\eta)$ become smaller. More heat

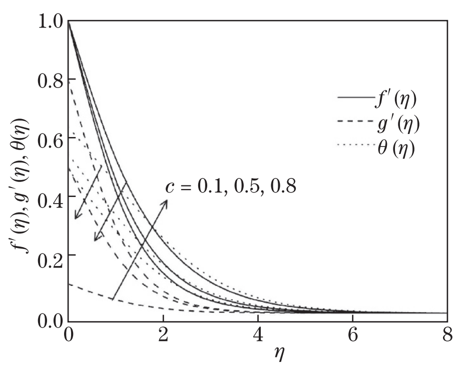

Fig. 3 Curves of $f'(\eta)$, $g'(\eta)$, and $\theta(\eta)$ for various c, where $\beta_1 = \beta_2 = 0.2$, $\lambda = 0.5$, $Pr = 1.2$, $R = 0.4$, $S = 0.3$, $Bi = 0.4$, and $\theta_w = 1.6$

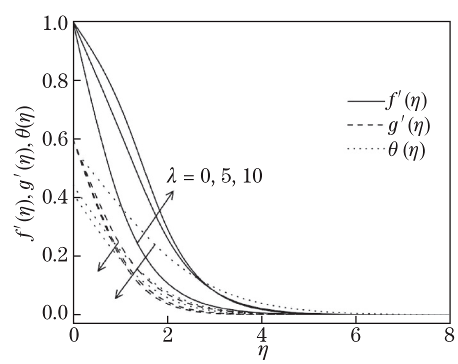

Fig. 4 Curves of $f'(\eta)$, $g'(\eta)$, and $\theta(\eta)$ for various values of λ, where $\beta_1 = \beta_2 = 0.2$, $c = 0.6$, $Pr = 1.2$, $R = 0.4$, $S = 0.3$, $Bi = 0.4$, and $\theta_w = 1.6$

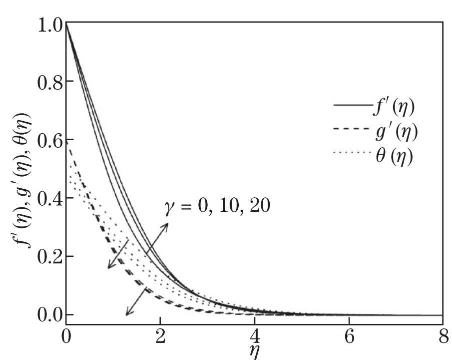

Fig. 5 Curves of $f'(\eta)$, $g'(\eta)$, and $\theta(\eta)$ for various values of γ, where $\beta_1 = \beta_2 = 0.2$, $\lambda = 0.5$, $c = 0.6$, $Pr = 1.2$, $R = 0.4$, $S = 0.3$, $Bi = 0.4$, and $\theta_w = 1.6$

is generated in the fluid due to the radiation that corresponds to the thicker momentum and the thermal boundary layer thicknesses. Similarly, an increase in the heat source/sink parameter leads to increases in the velocity $f'(\eta)$ and the temperature $\theta(\eta)$ and a decrease in the velocity $g'(\eta)$ (see Fig. 7). Here, $S = 0$ implies no heat source/sink, and $S > 0$ corresponds to heat source. The heat sink case occurs when the values of S are negative.

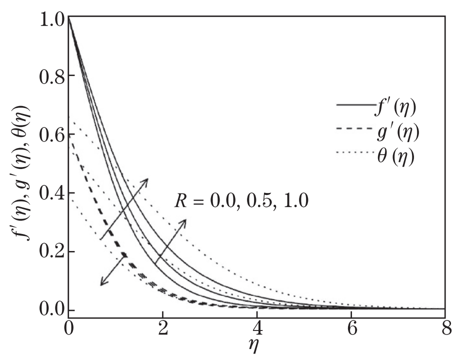

Fig. 6 Curves of $f'(\eta)$, $g'(\eta)$, and $\theta(\eta)$ for various values of R, where $\beta_1 = \beta_2 = 0.2$, $\lambda = 0.5$, $c = 0.6$, $Pr = 1.2$, $S = 0.3$, $Bi = 0.4$, and $\theta_w = 1.6$

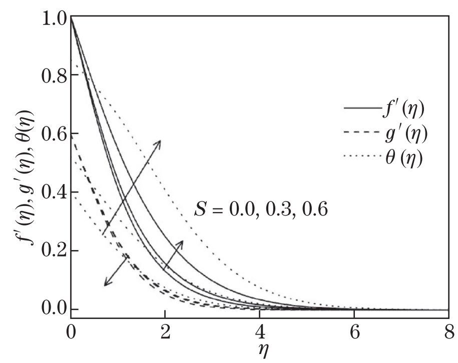

Fig. 7 Curves of $f'(\eta)$, $g'(\eta)$, and $\theta(\eta)$ for various values of S, where $\beta_1 = \beta_2 = 0.2$, $\lambda = 0.5$, $c = 0.6$, $Pr = 1.2$, $R = 0.4$, $Bi = 0.4$, and $\theta_w = 1.6$

The variations in $f'(\eta)$, $g'(\eta)$, and $\theta(\eta)$ corresponding to different values of the Biot number Bi are explored in Fig. 8. The variations in the curves of $g'(\eta)$ for multiple values of Bi are very small. The velocity $f'(\eta)$ and the temperature $\theta(\eta)$ are enhanced significantly due to an increase in Bi. The heat transfer coefficient becomes stronger for larger Bi, which gives rise to the fluid velocity $f'(\eta)$ and the temperature $\theta(\eta)$. The temperature ratio θ_w leads to remarkable changes in the curves of $f'(\eta)$ and $\theta(\eta)$, while the profile of $g'(\eta)$ changes very slowly (see Fig. 9).

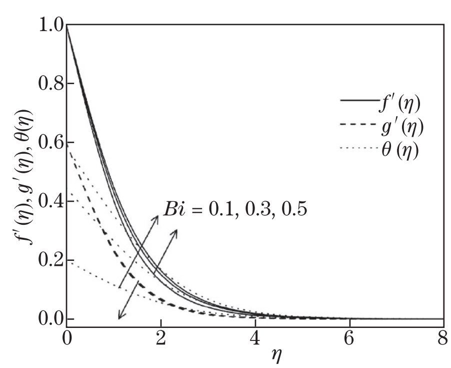

Fig. 8 Curves of $f'(\eta)$, $g'(\eta)$, and $\theta(\eta)$ for various values of Bi, where $\beta_1 = \beta_2 = 0.2$, $\lambda = 0.5$, $c = 0.6$, $Pr = 1.2$, $R = 0.4$, $S = 0.3$, and $\theta_w = 1.6$

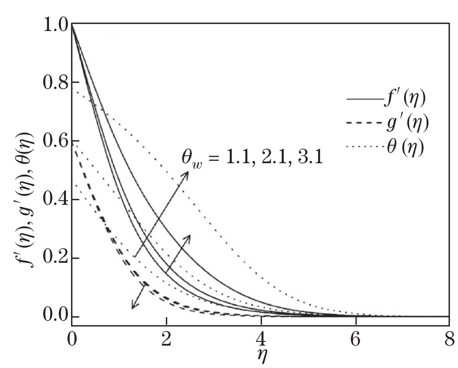

Fig. 9 Curves of $f'(\eta)$, $g'(\eta)$, and $\theta(\eta)$ for various values of θ_w, where $\beta_1 = \beta_2 = 0.2$, $\lambda = 0.5$, $c = 0.6$, $Pr = 1.2$, $R = 0.4$, $Bi = 0.4$, and $\gamma = 0.5$

The comparison of the present numerical results with those in Ref. [41] is made in Table 1. It is indicated that the present values of $f''(0)$ and $g''(0)$ for multiple values of c have an excellent match with the results of Ariel[41]. Table 2 is presented to examine the values of $f''(0)$, $g''(0)$, and $-(1+R\theta_w^3)\theta'(0)$ for multiple values of β_1 and β_2 when $c = 0.6$, $Pr = 1.2$, $S = 0.3$, $R = 0.4$,

Table 2 Numerical results of $f''(0)$, $g''(0)$, and $-(1+R\theta_w^3)\theta'(0)$ for different values of β_1 and β_2 when $c=0.6$, $Pr=1.2$, $S=0.3$, $R=0.4$, $\theta_w=1.6$, and $Bi=0.4$

		$\lambda=0,\ \gamma=0.5$			$\lambda=0.5,\ \gamma=0$			$\lambda=0.5,\ \gamma=0.5$		
β_1	β_2	$f''(0)$	$g''(0)$	$-(1+R\theta_w^3)$	$f''(0)$	$g''(0)$	$-(1+R\theta_w^3)$	$f''(0)$	$g''(0)$	$-(1+R\theta_w^3)$
0.0	0.0	–1.109 96	–0.590 54	0.443 90	–0.930 58	–0.601 45	0.498 70	–0.900 70	–0.602 63	0.502 21
0.1	0.1	–1.074 79	–0.570 19	0.448 87	–0.912 20	–0.583 09	0.497 57	–0.884 86	–0.584 48	0.500 71
0.2	0.1	–1.118 40	–0.592 84	0.406 81	–0.942 54	–0.609 70	0.478 30	–0.912 60	–0.611 51	0.482 17
0.3	0.1	–1.160 70	–0.614 71	0.350 39	–0.970 89	–0.636 02	0.458 78	–0.938 18	–0.638 32	0.463 51
0.4	0.1	–1.201 76	–0.635 87	0.266 87	–0.997 62	–0.662 06	0.439 32	–0.962 02	–0.664 90	0.444 98
0.2	0.05	–1.159 87	–0.615 40	0.372 25	–0.967 12	–0.633 91	0.467 91	–0.934 24	–0.635 91	0.472 45
0.2	0.1	–1.118 40	–0.592 84	0.406 81	–0.942 54	–0.609 70	0.478 30	–0.912 60	–0.611 51	0.482 17
0.2	0.15	–1.081 10	–0.572 60	0.432 34	–0.919 65	–0.587 99	0.487 73	–0.892 24	–0.589 63	0.491 05
0.2	0.2	–1.047 30	–0.554 30	0.452 18	–0.898 26	–0.568 38	0.496 29	–0.873 05	–0.569 88	0.499 16

$\theta_w=1.6$, and $Bi=0.4$. Here, we have computed the values by considering $\lambda=0$ and $\gamma=0.5$, $\lambda=\gamma=0.5$, and $\lambda=0.5$ and $\gamma=0$. From Table 2, we can see that the values of $f''(0)$ and $-(1+R\theta_w^3)\theta'(0)$ when $\lambda=0$ and $\gamma=0.5$ or $\lambda=0.5$ and $\gamma=0$ are smaller than those when $\lambda=\gamma=0.5$, while the values of $g''(0)$ when $\lambda=0$ and $\gamma=0.5$ or $\lambda=0.5$ and $\gamma=0$ are bigger than those when $\lambda=\gamma=0.5$. It can be also seen that the values of $f''(0)$ and $g''(0)$ decay with an enhancement in β_1 while boost up with an increase in β_2. The values of $-(1+R\theta_w^3)\theta'(0)$ are enhanced for larger β_1, while decrease when β_2 increases.

The values of $f''(0)$, $g''(0)$, and $-(1+R\theta_w^3)\theta'(0)$ for different values of R by setting

$$c=0.6,\quad Pr=1.2,\quad S=0.3,\quad \beta_1=0.2=\beta_2,\quad \theta_w=1.6,\quad Bi=0.4$$

are investigated in Table 3. In this Table, we make an analysis of the values of $f''(0)$, $g''(0)$, and $-(1+R\theta_w^3)\theta'(0)$ in absence of radiation, linear radiation, and non-linear radiation. The results show that the radiation term has no effect on the values of $f''(0)$ and $g''(0)$ when $\lambda=0$, and $\gamma=0.5$. The numerical values of $-(1+R\theta_w^3)\theta'(0)$ are larger in the non-linear radiation situation than those in the cases of linear radiation and absence of radiation. In Table 4, we have studied the values of $f''(0)$, $g''(0)$, and $-(1+R\theta_w^3)\theta'(0)$ for various values of Bi by setting

$$c=0.6,\quad Pr=1.2,\quad S=0.3,\quad \beta_1=0.2=\beta_2,\quad \theta_w=1.6,\quad \lambda=0.5,\quad \gamma=1.0.$$

Here, we notice that smaller values of the Biot number have greater effects on the values of $f''(0)$, $g''(0)$, and $-(1+R\theta_w^3)\theta'(0)$.

Table 3 Numerical results of $f''(0)$, $g''(0)$, and $-(1+R\theta_w^3)\theta'(0)$ for different values of R when $c=0.6$, $Pr=1.2$, $S=0.3$, $\beta_1=\beta_2=0.2$, $Bi=0.4$, $\lambda=0.5$, and $\gamma=1$

		$\lambda=0,\ \gamma=0.5$			$\lambda=0.5,\ \gamma=0$			$\lambda=0.5,\gamma=0.5$		
Case	R	$f''(0)$	$g''(0)$	$-(1+R\theta_w^3)$	$f''(0)$	$g''(0)$	$-(1+R\theta_w^3)$	$f''(0)$	$g''(0)$	$-(1+R\theta_w^3)$
Absence of radiation	0.0	–1.047 30	–0.554 30	0.239 97	–0.962 93	–0.560 60	0.242 88	–0.952 19	–0.561 10	0.243 08
Linear radiation	0.2	–1.047 30	–0.554 30	0.267 14	–0.944 92	–0.562 79	0.273 45	–0.930 78	–0.563 52	0.243 08
	0.4	–1.047 30	–0.554 30	0.287 74	–0.927 02	–0.565 12	0.300 05	–0.909 28	–0.566 11	0.273 87
	0.6	–1.047 30	–0.554 30	0.301 90	–0.909 76	–0.567 47	0.323 50	–0.888 38	–0.568 74	0.300 83
	0.8	–1.047 30	–0.554 30	0.310 24	–0.893 57	–0.569 75	0.344 57	–0.868 58	–0.571 31	0.324 78
Non-linear radiation	0.2	–1.047 30	–0.554 30	0.293 71	–0.941 28	–0.563 17	0.301 52	–0.926 28	–0.563 95	0.346 48
	0.4	–1.047 30	–0.554 30	0.332 44	–0.919 36	–0.565 97	0.350 22	–0.899 72	–0.567 09	0.302 05
	0.6	–1.047 30	–0.554 30	0.355 92	–0.898 06	–0.568 85	0.390 98	–0.873 60	–0.570 33	0.351 36
	0.8	–1.047 30	–0.554 30	0.364 92	–0.878 03	–0.571 65	0.425 72	–0.848 81	–0.573 52	0.393 06

Table 4 Numerical results of $f''(0)$, $g''(0)$, and $-(1+R\theta_w^3)\theta'(0)$ for different values of Bi when $c=0.6$, $Pr=1.2$, $S=0.3$, $\beta_1=\beta_2=0.2$, $Bi=0.2$, $\theta_w=1.6$, $\lambda=0.5$, and $\gamma=1$

Bi	$\beta_1=\beta_2=0$			$\beta_1=\beta_2=0.2$		
	$f''(0)$	$g''(0)$	$-(1+R\theta_w^3)\theta'(0)$	$f''(0)$	$g''(0)$	$-(1+R\theta_w^3)\theta'(0)$
0.2	–0.967 56	–0.598 80	0.239 63	–0.960 16	–0.561 36	0.256 98
0.5	–0.836 95	–0.605 48	0.381 66	–0.873 00	–0.567 73	0.436 10
0.9	–0.746 81	–0.609 82	0.455 33	–0.806 19	–0.572 37	0.542 42
2.0	–0.651 32	–0.614 27	0.519 09	–0.727 92	–0.577 63	0.643 86
5.0	–0.589 30	–0.617 08	0.554 61	–0.672 57	–0.581 27	0.704 27
10	–0.565 84	–0.618 14	0.567 04	–0.650 70	–0.582 69	0.726 04
100	–0.543 40	–0.619 14	0.578 48	–0.629 30	–0.584 07	0.746 32
500	–0.541 35	–0.619 23	0.579 51	–0.627 32	–0.584 20	0.748 15
1 000	–0.541 09	–0.619 24	0.579 64	–0.627 07	–0.584 22	0.748 38
10 000	–0.540 85	–0.619 25	0.579 75	–0.626 85	–0.584 23	0.748 59
100 000	–0.540 83	–0.619 25	0.579 77	–0.626 82	–0.584 23	0.748 61
1 000 000	–0.540 83	–0.619 25	0.579 77	–0.626 82	–0.584 23	0.748 61

5 Conclusions

The role of non-linear convection and thermal radiation in the three-dimensional flow of the Oldroyd-B liquid is explored. The heat transfer phenomenon is examined under the heat source/sink and convective surface condition. Numerical computations have been carried out to analyze the solutions of the velocities and temperature. The results show that the Deborah numbers β_1 and β_2 have reverse effects on the velocities and temperature. It is also noted that the values of the velocity $f'(\eta)$ at the wall are higher than the values of the velocity $g'(\eta)$ and the temperature $\theta(\eta)$. Larger c leads to smaller $f'(\eta)$ while bigger $g'(\eta)$. The velocity $f'(\eta)$ is an increasing function of the mixed convection parameter. When the non-linear convection parameter γ increases, the velocity $g'(\eta)$ and the temperature $\theta(\eta)$ decrease. The temperature $\theta(\eta)$ increases significantly when Bi increases. The values of $f''(0)$ and $-(1+R\theta_w^3)\theta'(0)$ when $\lambda=0$ and $\gamma=0.5$ or $\lambda=0.5$ and $\gamma=0$ are smaller than those when $\lambda=\gamma=0.5$. The values of $g''(0)$ when $\lambda=0$ and $\gamma=0.5$ or $\lambda=0.5$ and $\gamma=0$ are bigger than those when $\lambda=\gamma=0.5$. The results also show that the radiation term has no effect on the values of $f''(0)$ and $g''(0)$ when $\lambda=0$, and $\gamma=0.5$. The numerical values of $-(1+R\theta_w^3)\theta'(0)$ in the case of non-linear radiation are larger than those in the cases of linear radiation and absence of radiation. It is noticed that smaller values of the Biot number have greater effects on the values of $f''(0)$, $g''(0)$, and $-(1+R\theta_w^3)\theta'(0)$.

References

[1] Sajid, M., Abbas, Z., Javed, T., and Ali, N. Boundary layer flow of an Oldroyd-B fluid in the region of a stagnation point over a stretching sheet. *Canadian Journal of Physics*, **88**, 635–640 (2010)

[2] Shehzad, S. A., Alsaedi, A., Hayat, T., and Alhuthali, M. S. Three-dimensional flow of an Oldroyd-B fluid with variable thermal conductivity and heat generation/absorption. *PLoS One*, **8**, e78240 (2013)

[3] Hayat, T., Hussain, Z., Farooq, M., Alsaedi, A., and Obaid, M. Thermally stratified stagnation point flow of an Oldroyd-B fluid. *International Journal of Nonlinear Sciencesand Numerical Simulation*, **15**, 77–86 (2014)

[4] Motsa, S. S., Makukula, Z. G., and Shateyi, S. Numerical investigation of the effect of unsteadiness on three-dimensional flow of an Oldroyd-B fluid. *PLoS One*, **10**, e0133507 (2015)

[5] Abbasi, F. M., Mustafa, M., Shehzad, S. A., Alhuthali, M. S., and Hayat, T. Analytical study of Cattaneo-Christov heat flux model for a boundary layer flow of Oldroyd-B fluid. *Chinese Physics B*, **25**, 014701 (2016)

[6] Sheikholeslami, M., Gorji-Bandpy, M., and Ganji, D. D. Lattice Boltzmann method for MHD natural convection heat transfer using nanofluid. *Powder Technology*, **254**, 82–93 (2014)

[7] Sheikholeslami, M., Rashidi, M. M., and Ganji, D. D. Effect of non-uniform magnetic field on forced convection heat transfer of Fe_3O_4-water nanofluid. *Computers Methods in Applied Mechanics and Engineering*, **294**, 299–312 (2015)

[8] Mahanthesh, B., Gireesha, B. J., and Gorla, R. S. R. Mixed convection squeezing three-dimensional flow in a rotating channel filled with nanofluid. *International Journal of Numerical Methods for Heat & Fluid Flow*, **26**, 1460–1485 (2016)

[9] Rashidi, M. M., Nasiri, M., Khezerloo, M., and Laraqi, N. Numerical investigation of magnetic field effect on mixed convection heat transfer of nanofluid in a channel with sinusoidal walls. *Journal of Magnetism and Magnetic Materials*, **401**, 159–168 (2016)

[10] Abbasi, F. M., Shehzad, S. A., Hayat, T., and Ahmad, B. Doubly stratified mixed convection flow of Maxwell nanofluid with heat generation/absorption. *Journal of Magnetism and Magnetic Materials*, **404**, 159–165 (2016)

[11] Shehzad, S. A., Hayat, T., Alsaedi, A., and Ahmad, B. Effects of thermophoresis and thermal radiation in mixed convection three-dimensional flow of Jeffrey fluid. *Applied Mathematics and Mechanics* (*English Edition*), **36**(5), 655–668 (2015) DOI 10.1007/s10483-015-1935-7

[12] Zhao, N. and Iramina, K. Numerical simulation of effect of convection-diffusion on oxygen transport in microcirculation. *Applied Mathematics and Mechanics* (*English Edition*), **36**(2), 179–200 (2015) DOI 10.1007/s10483-015-1908-7

[13] Hayat, T., Qayyum, A., and Alsaedi, A. Three-dimensional mixed convection squeezing flow. *Applied Mathematics and Mechanics* (*English Edition*), **36**(1), 47–60 (2015) DOI 10.1007/s10483-015-1894-9

[14] Zhao, Q., Xu, H., Tao, L., Raees, A., and Sun, Q. Three-dimensional free bio-convection of nanofluid near stagnation point on general curved isothermal surface. *Applied Mathematics and Mechanics* (*English Edition*), **37**(4), 417–432 (2016) DOI 10.1007/s10483-016-2046-9

[15] Cao, L., Si, X., and Zheng, L. Convection of Maxwell fluid over stretching porous surface with heat source/sink in presence of nanoparticles: Lie group analysis. *Applied Mathematics and Mechanics* (*English Edition*), **37**(4), 433–442 (2016) DOI 10.1007/s10483-016-2052-9

[16] Makinde, O. D. Free convection flow with thermal radiation and mass transfer past a moving vertical porous plate. *International Communications in Heat and Mass Transfer*, **32**, 1411–1419 (2005)

[17] Su, X., Zheng, L., Zhang, X., and Zhang, J. MHD mixed convective heat transfer over a permeable stretching wedge with thermal radiation and ohmic heating. *Chemical Engineering Science*, **78**, 1–8 (2012)

[18] Gireesha, B. J. and Mahanthesh, B. Perturbation solution for radiating viscoelastic fluid flow and heat transfer with convective boundary condition in non-uniform channel with Hall current and chemical reaction. *Thermodynamics*, **2013**, 935481 (2013)

[19] Shehzad, S. A., Alsaadi, F. E., Hayat, T., and Monaquel, S. J. MHD mixed convection flow of thixotropic fluid with thermal radiation. *Heat Transfer Research*, **45**, 659–676 (2014)

[20] Lin, Y., Zheng, L., and Zhang, X. Radiation effects on Marangoni convection flow and heat transfer in pseudo-plastic non-Newtonian nanofluids with variable thermal conductivity. *International Journal of Heat and Mass Transfer*, **77**, 708–716 (2014)

[21] Rashidi, M. M., Ganesh, N. V., Hakeem, A. K. A., and Ganga, B. Buoyancy effect on MHD flow of nanofluid over a stretching sheet in the presence of thermal radiation. *Journal of Molecular Liquids*, **198**, 234–238 (2014)

[22] Gireesha, B. J., Gorla, R. S. R., and Mahanthesh, B. Effect of suspended nanoparticles on three-dimensional MHD flow, heat and mass transfer of radiating Eyring-Powell fluid over a stretching sheet. *Journal of Nanofluids*, **4**, 474–484 (2015)

[23] Zhang, C., Zheng, L., Zhang, X., and Chen, G. MHD flow and radiation heat transfer of nanofluids in porous media with variable surface heat flux and chemical reaction. *Applied Mathematical Modelling*, **39**, 165–181 (2015)

[24] Hayat, T., Waqas, M., Shehzad, S. A., and Alsaedi, A. A model of solar radiation and Joule heating in magnetohydrodynamic (MHD) convective flow of thixotropic nanofluid. *Journal of Molecular Liquids*, **215**, 704–710 (2016)

[25] Sheikholeslami, M., Hayat, T., and Alsaedi, A. MHD free convection of Al_2O_3-water nanofluid considering thermal radiation: a numerical study. *International Journal of Heat and Mass Transfer*, **96**, 513–524 (2016)

[26] Cortell, R. Fluid flow and radiative nonlinear heat transfer over a stretching sheet. *Journal of King Saud University of Sciences*, **26**, 161–167 (2014)

[27] Mushtaq, A., Mustafa, M., Hayat, T., and Alsaedi, A. Nonlinear radiative heat transfer in the flow of nanofluid due to solar energy: a numerical study. *Journal of the Taiwan Institute of Chemical Engineers*, **45**, 1176–1183 (2014)

[28] Shehzad, S. A., Hayat, T., Alsaedi, A., and Obid, M. A. Nonlinear thermal radiation in three-dimensional flow of Jeffrey nanofluid: a model for solar energy. *Applied Mathematics and Computation*, **248**, 273–286 (2014)

[29] Hayat, T., Muhammad, T., Alsaedi, A., and Alhuthali, M. S. Magnetohydrodynamic three-dimensional flow of viscoelastic nanofluid in the presence of nonlinear thermal radiation. *Journal of Magnetism and Magnetic Materials*, **385**, 222–229 (2015)

[30] Mahanthesh, B., Gireesha, B. J., and Gorla, R. S. R. Nonlinear radiative heat transfer in MHD three-dimensional flow of water based nanofluid over a non-linearly stretching sheet with convective boundary condition. *Journal of Nigerian Mathematical Society*, **35**, 178–198 (2016)

[31] Sheikholeslami, M., Ganji, D. D., Ashorynejad, H. R., and Rokni, H. B. Analytical investigation of Jeffery-Hamel flow with high magnetic field and nanoparticle by Adomian decomposition method. *Applied Mathematics and Mechanics* (*English Edition*), **33**(1), 25–36 (2012) DOI 10.1007/s10483-012-1531-7

[32] Sheikholeslami, M., Gorji-Bandpy, M., and Domairry, G. Free convection of nanofluid filled enclosure using lattice Boltzmann method (LBM). *Applied Mathematics and Mechanics* (*English Edition*), **34**(7), 833–846 (2013) DOI 10.1007/s10483-013-1711-9

[33] Kandelousi, M. S. KKL correlation for simulation of nanofluid flow and heat transfer in a permeable channel. *Physics Letters A*, **378**, 3331–3339 (2014)

[34] Kandelousi, M. S. Effect of spatially variable magnetic field on ferrofluid flow and heat transfer considering constant heat flux boundary condition. *The European Physical Journal Plus*, **129**, 248 (2014)

[35] Sheikholeslami, M. CVFEM for magnetic nanofluid convective heat transfer in a porous curved enclosure. *The European Physical Journal Plus*, **131**, 413 (2016)

[36] Sheikholeslami, M. Magnetic field influence on nanofluid thermal radiation in a cavity with tilted elliptic inner cylinder. *Journal of Molecular Liquids*, **229**, 137–147 (2017)

[37] Sheikholeslami, M. and Chamkha, A. J. Influence of Lorentz forces on nanofluid forced convection considering Marangoni convection, *Journal of Molecular Liquids*, **225**, 750–757 (2017)

[38] Sheikholeslami, M. Numerical simulation of magnetic nanofluid natural convection in porous media. *Physics Letters A*, **381**, 494–503 (2017)

[39] Sheikholeslami, M. and Rokni, H. B. Nanofluid two phase model analysis in existence of induced magnetic field. *International Journal of Heat and Mass Transfer*, **107**, 288–299 (2017)

[40] Sheikholeslami, M. and Vajravelu, K. Nanofluid flow and heat transfer in a cavity with variable magnetic field. *Applied Mathematics and Computation*, **298**, 272–282 (2017)

[41] Ariel, P. D. The three-dimensional flow past a stretching sheet and the homotopy perturbation method. *Computers & Mathematics with Applications*, **54**, 920–925 (2007)